PROCEEDINGS OF SCIENCE

Helium flux and its ratio to proton flux in cosmic rays measured with CALET on the International Space Station

Paolo Brogi[a,b,*] **and K. Kobayashi**[c,d] **for the CALET collaboration**

[a] *INFN Sezione di Pisa, Polo Fibonacci, Largo B. Pontecorvo, 3, 56127 Pisa, Italy*

[b] *Department of Physical Sciences, Earth and Environment, University of Siena, via Roma 56, 53100 Siena, Italy*

[c] *Waseda Research Institute for Science and Engineering, Waseda University, 17 Kikuicho, Shinjuku, Tokyo 162-0044, Japan*

[d] *JEM Utilization Center, Human Spaceflight Technology Directorate, Japan Aerospace Exploration Agency, 2-1-1 Sengen, Tsukuba, Ibaraki 305-8505, Japan*

E-mail: paolo.brogi@unisi.it

The CALorimetric Electron Telescope (CALET) is a space-based calorimetric instrument, designed to carry out precision measurements of high energy cosmic rays. Installed on the Japanese Experiment Module – Exposed Facility on the ISS, it is collecting data with excellent performance and no significant interruptions since October 2015. We present the results of a direct measurement of the energy spectrum of cosmic-ray helium, based on about 6.5 years of collected data. It shows significant deviations from a single power law with a progressive hardening around a few hundred GeV followed by a softening in the multi-TeV region. A measurement of the proton to helium flux ratio is also presented. Thanks to the recent update of the CALET proton flux with higher statistics, the p/He ratio is measured with high precision, extending the energy reach of previous measurements with magnetic spectrometers by more than one order of magnitude.

38th International Cosmic Ray Conference (ICRC2023)
26 July - 3 August, 2023
Nagoya, Japan

*Speaker

1. Introduction

The CALorimetric Electron Telescope (CALET) is a space-based experiment developed and operated by an international collaboration led by the Japanese Space Agency (JAXA) with the participation of the Italian Space Agency (ASI) and NASA. The CALET detector was installed on the Japanese Experiment Module Exposure Facility (JEM-EF) onboard the International Space Station (ISS) since August 2015, and after a preliminary commissioning phase, it is taking data smoothly from October 2015.
The CALET science program is wide and addresses several outstanding questions of high-energy astroparticle physics including the origin of cosmic rays (CR); the possible presence of nearby astrophysical CR sources; the study of their acceleration mechanism(s); the propagation of primary and secondary elements in the galaxy; the nature of dark matter and its localization. Moreover, the CALET telescope is also capable to detect gamma-ray transients trough a dedicated instrument (CGBM) that covers the energy range 7 keV – 20 MeV, and could be used, in combination with the calorimeter, to perform the search of counterpart emission related to gravitational wave events [1, 2]. Taking advantage of its wide dynamic range, large thickness and excellent charge identification capability, CALET is carrying out extensive measurements of individual chemical elements in CR up to nickel, in the energy range from few GeV up to the PeV region.
In this paper, we describe the analysis procedure for the Helium flux measurement (preliminarily reported in [3]), and we present the results based on the data collected in 2392 days of CALET operation onboard the ISS, recently published in [4].

2. The CALET telescope

The CALET main telescope, is an all-calorimetric instrument, that consists of three sub-detectors.

The CHarge Detector (CHD), that is positioned at the top of the apparatus and consists of a two layer hodoscope of plastic scintillators paddles (14 paddles for each layer): this first sub-detector performs the charge identification of individual nuclear species, providing a measurement of the charge Z of the incident particle over a wide dynamic range (from $Z = 1$ up to $Z = 40$). The IMaging Calorimeter (IMC), a fine grained sampling calorimeter segmented longitudinally into 16 layers of scintillating fibers (with 1 mm^2 square cross-section) read out individually and arranged in pairs along orthogonal directions, each pair is interleaved with thin tungsten absorbers (for a total thickness of $3X_0$). It is used to reconstruct the early shower profile and the impinging particle trajectory with good angular resolution and a redundant charge measurement [5]. The third detector is the Total AbSorption Calorimeter (TASC), an homogeneous calorimeter made of 12 layers of lead-tungstate (PWO) logs, arranged in pairs along $x - y$ directions, and capable, with its 27 X_0 thickness and its shower imaging capability, to measure electrons and gamma-rays with an excellent energy resolution, providing high discrimination against hadronic cascades.
The total thickness of the main telescope is equivalent to 30 X_0 and 1.3 proton interaction lengths (λ_I), the geometrical factor is 0.12 m^2 sr. A more detailed description of the instrument can be found in [6] and in the Supplemental Material (SM) of [7].

3. Data analysis

In the analysis reported here, we use 2392 days of flight data (FD) collected from October 13, 2015 to April 30, 2022.

The raw signal of each detector channel is carefully calibrated using penetrating protons and He particles, selected in-flight by a dedicated trigger mode in order to correct for non-uniformity in light output, gain differences among the channels, position, temperature and temporal gain variations [6]. For each CR event the impinging particle track, charge and energy are then reconstructed. This allows to select the helium sample, sorted into energy intervals, in order to compute the energy spectrum. Two detailed Monte Carlo (MC) simulations, based on EPICS and FLUKA [8] packages were developed, they are used to validate and tune the reconstruction method and evaluate event reconstruction efficiencies, background contaminations and the energy response matrix. The whole analysis it is carefully described here [4], in the following subsections we report the main steps of the procedure.

3.1 Preselection

Well reconstructed and contained events were selected on the basis of the following criteria: **Trigger:** the on-board high-energy (HE) trigger mode, used for this analysis, is designed to ensure maximum exposure to electrons above 10 GeV and other high-energy shower events. An offline trigger confirmation is applied, requiring sufficiently more severe conditions than the HE trigger, to avoid position, temperature and temporal gain variations. **Track quality cut:** only well reconstructed trucks using a combinatorial Kalman Filter (KF) algorithm [9] are selected. A minimum number of points are required for each track segment, and a χ^2 cut is applied. For He nuclei we achieve an angular resolution of about 0.1°and a resolution on the CHD of ~400 μm. **Geometrical condition:** The reconstructed events are required to pass through the whole detector, i.e., from CHD top to TASC bottom, with 2 cm clearance from the edges of the TASC top layer. Within a fiducial region, known as acceptance A1, limited to a Geometric Factor of 0.051 $m^2 sr$ (~49% of the total GF). **Electron rejection:** This cut is based on the energy deposits found inside one Moliere radius around each IMC fiber matched to the track and on the energy deposit in the last TASC layer. Most of the electrons are rejected while retaining a very high efficiency for helium nuclei (> 99.9% for $E > 50$ GeV). **Off-Acceptance Rejection (OAR) cuts:** Due to the occasional misidentification of one of the secondary tracks as the primary track. A number of events are erroneously reconstructed inside the fiducial acceptance A1, while the true acceptance is different. To reject most of these events, different topological cuts are applied using the TASC information.

3.2 Charge identification

In CALET, the charge is measured with two independent subsystems that are routinely used to cross-calibrate each other: the CHD and the IMC. The tracking information is used to select the CHD paddles crossed by the primary particle, the information from the two CHD layers is combined into a single charge estimator. The IMC, being equipped with individually readout scintillating fibers, has a suitable granularity not only to provide excellent tracking capabilities, but also to sample the ionization deposits along the track in each layer, providing an alternative charge estimator through multiple dE/dx measurement. Both charge measurements are calibrated and

corrected for several effects: position, time-dependence, non-linear response due to the saturation of the scintillation light, energy shift related to the back-splash background increasing with energy. Then, to have a perfect agreement between the flight data (FD) and MC, the MC data are fine tuned over FD. An energy dependent charge cut, on both the charge estimator, is used to select the Helium nuclei among the other nuclear species, this allows to obtain an almost flat charge selection efficiency (roughly 65%). See [4] and its Supplemental Material (SM) for details.

3.3 Background subtraction

Background contamination is estimated from the MC simulation of protons, helium and from FD, as a function of the observed energy. Available spectral data, e.g. from [10–12], are used to simulate their spectral shape. The MC simulations are used to evaluate the relative contributions, and the FD to assess the proton and helium relative abundances. The dominant component is the charge contamination from protons misidentified as helium. Other not negligible contributions are from off-acceptance helium and protons mis-reconstructed inside acceptance A1. The estimated background is then subtracted bin by bin from the measured helium candidate distribution (dN/dE), prior to the unfolding procedure used to reconstruct the primary particle energy starting from the measured shower energy in TASC.

3.4 Energy measurement

The shower energy of each event is calculated as the sum of the calibrated energy deposits of all the TASC channels. Unlike for electrons, the energy released in TASC by interacting CR nuclei is only a fraction of the primary particle energy with large event-to-event fluctuations. For flux measurement, energy unfolding is applied by means of an iterative unfolding method based on the Bayes theorem [13], to correct dN/dE distribution of selected helium candidates for significant bin-to-bin migration effects (due to the limited energy resolution) and infer the primary particle energy. The energy bin width is chosen commensurate with the RMS resolution of TASC (30% for nuclei).

3.5 Systematic evaluation

The sources of systematic uncertainties in helium analysis can be grouped into energy independent and energy dependent contributions. The former include systematic effects in normalization that were studied in details here [7] and is estimated as 4.1%. The latter includes the following contributions. **Trigger:** the absolute calibration of the trigger efficiency was performed at the beam test. The main source of uncertainty comes from the accuracy of the calibration. Possible systematic bias due to normalization in the measurements of trigger efficiency was considered as uncertainty. **Shower energy correction:** as in the case of the uncertainty on the trigger efficiency, the absolute calibration of the energy response was performed using the beam test data in the low-energy region. Both the contribution coming from the accuracy of the calibration and from the model used to fit the test beam data are taken into account to assess this systematic. **Track reconstruction and acceptance:** tracking can affect many aspects of the analysis, the effects on the flux are evaluated by studying its dependence on pre-selection cuts relative to goodness-of-tracking. To investigate the uncertainty on the acceptance, restricted acceptance regions have been studied

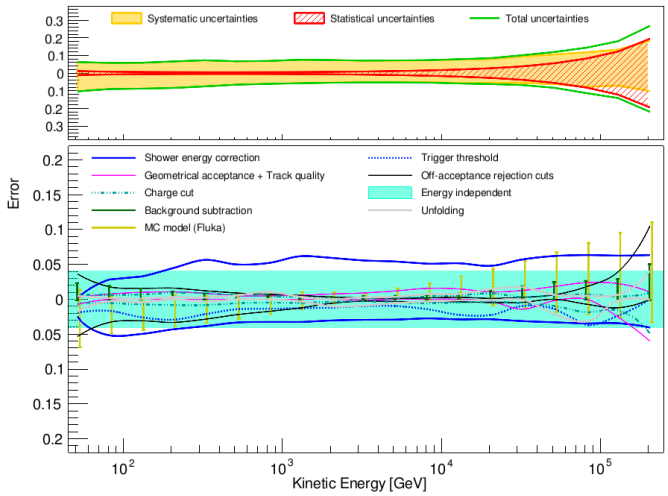

Figure 1: Breakdown of the systematic uncertainties evaluated in this analysis (see SM of [4] for details). Each colored line represent a different systematic, the total systematic error is shown by the solid green band. The red hatched area represent the statistical error.

and the resultant fluxes compared. **Background subtraction:** background subtraction is found to be slightly dependent from the simulated spectral shape, several re-weighting function were adopted to vary the MC spectrum, the relative differences with respect to the reference case were considered as systematic uncertainty for each energy bin. **Unfolding:** the uncertainties from the unfolding procedure were evaluated by applying different response matrices computed by varying the spectral index of the MC generation spectrum, or the number of iterations of the Bayesian method. **Charge ID and Off-Acceptance Rejection cuts:** The thresholds of each cut has been varied separately in a reasonable range around the reference value (1 FWHM), and the differences between the reference case and all the other cases were considered as systematic uncertainty. **MC model:** we have performed a detailed evaluation of the systematic uncertainty related to the MC model using a second Monte Carlo (i.e. Fluka) to compare with the adopted one (Epics). For each bin, this systematic error is obtained using Fluka instead of EPICS to evaluate: the shower energy correction, the smearing matrix, and all relevant selection efficiencies.

Two independent helium analyses were carried out by separate groups inside the CALET collaboration, using different event selection and background rejection procedure, preliminary results are consistent within the errors.

4. Helium energy spectrum and p/He ratio

The helium energy spectrum is calculated as: $\Phi(\tilde{E}) = \dfrac{N(E)}{\Delta E \times \varepsilon(E) \times \Omega \times LT}$ where $\tilde{E}$ is the median kinetic energy of the $[E, E + \Delta E)$ bin, ΔE is the energy bin width, $\varepsilon(E)$ the overall selection efficiency, and LT is the live time ($\sim 85\%$ of total observation time), Ω the "fiducial" geometrical acceptance ($\sim 510\ cm^2 sr$), $N(E)$ the bin content in the unfolded distribution.

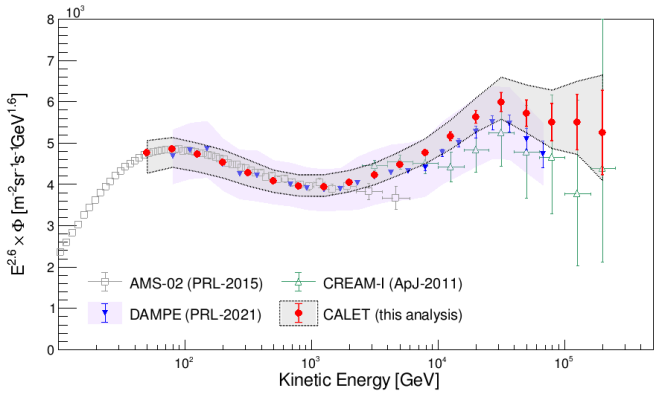

Figure 2: Helium flux measurement with CALET [4] (red markers), compared with previous direct observations [11, 12, 14]. The error bars represent only the statistical error; the gray band represents the quadratic sum of statistical and systematic error. The light violet colored band shows the systematic uncertainty of [14].

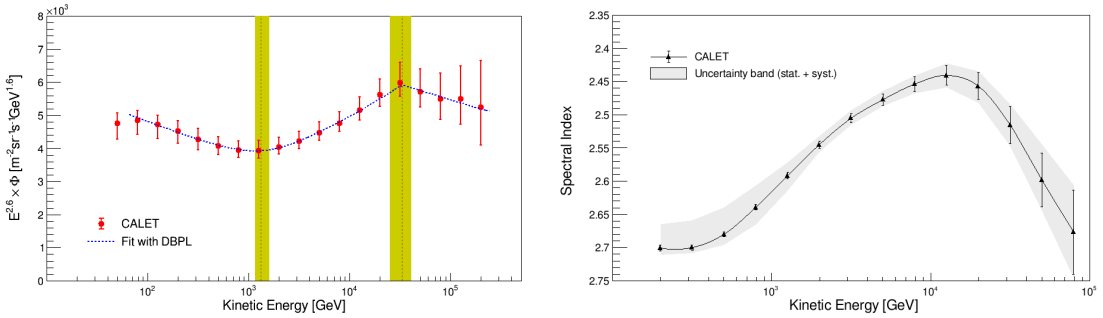

Figure 3: Left panel: fit of CALET data with a DBPL function [4]. Both statistical and systematic uncertainties are taken into account. Right panel: energy dependence of the spectral index calculated within a sliding energy window for CALET data [4]. The gray band indicates the uncertainty range including systematics.

The energy spectrum of helium nuclei in CR, as measured with CALET in 2392 days of operation [4] is shown in figure 2 covering an interval of kinetic energy per particle from ∼40 GeV to ∼250 TeV, compared with previous observations from space-based [12, 14] and balloon-borne [11] experiments. Our spectrum is in good agreement with the very accurate measurements by AMS-02 in the lower energy region below a few TeV, as well as with the measurements from calorimetric instruments in the higher energy region, in particular with the recent measurement of DAMPE [14]. A fit of CALET data has been performed using a "double smoothly broken power-law" [4], in the energy range from 60 GeV to 250 TeV, and is reported in the left panel of figure 3. A progressive hardening up to the multi-TeV region was observed, and the fit gives a power law index (γ), $\Delta\gamma$ and break energy (E_0) consistent, within the errors, with the most recent results of DAMPE [14]. A progressive hardening from a few hundred GeV to a few tens TeV and the onset of a flux softening above a few tens of TeV are observed. The fit returns a power law index $\gamma = -2.703\ ^{+0.005}_{-0.006}\ (stat)\ ^{+0.032}_{-0.009}\ (syst)$, $\Delta\gamma = 0.25\ ^{+0.02}_{-0.01}\ (stat)\ ^{+0.02}_{-0.03}\ (syst)$, first break energy

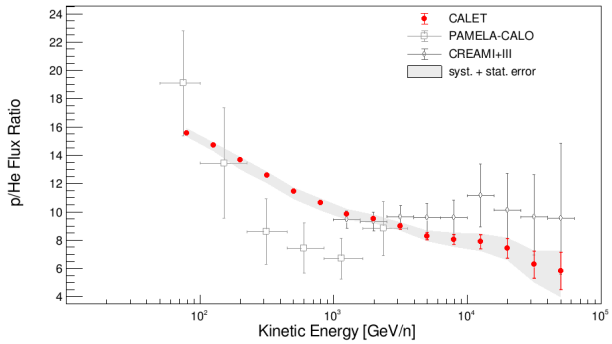

Figure 4: p/He ratio measurement with CALET [4] (red markers), compared with previous direct observations [17]. The error bars represent only statistical error, the gray band represents statistical and systematic error.

$E_0 = 1319\ ^{+113}_{-93}\ (stat)\ ^{+267}_{-124}\ (syst)$ GeV and smoothness parameter $S = 2.7\ ^{+0.6}_{-0.5}\ (stat)\ ^{+3.0}_{-0.9}\ (syst)$, with a second spectral index variation $\Delta\gamma_1 = -0.22\ ^{+0.07}_{-0.10}\ (stat)\ ^{+0.03}_{-0.04}\ (syst)$ and second break energy $E_1 = 33.2\ ^{+9.8}_{-6.2}\ (stat)\ ^{+1.8}_{-2.3}\ (syst)$ TeV. Given the relatively large uncertainties of the data in the highest energy bins, the second smoothness parameter S_1 cannot be effectively constrained and is kept fixed at value $S_1 = 30$. The index change $\Delta\gamma$ is proven to be different from zero by more than 8 σ, taking into account both statistical and systematic error [4]. The fit parameters are generally consistent, within the errors, with the recent results of DAMPE [14], although $\Delta\gamma_1$ seems to indicate a less pronounced softening in our data. The spectral hardening and softening can be easily seen also in the right panel of figure 3, where the spectral index is shown as a function of kinetic energy [4]. The black marker in the plot represents the index γ with its statistical error, while the gray band represents the quadratic sum of statistical end systematic uncertainties.

Differences between the proton and helium spectra can contribute important constraints on acceleration models. To ease the comparison we have calculated the helium spectrum (from this analysis) in kinetic energy per nucleon [4] and the proton over He flux ratio. The ^{3}He contribution to the flux has been taken into account assuming the AMS-02 [15] measurement of the ^{3}He/^{4}He ratio and extrapolating it to higher energies with use of a single power-law fit. The p/He flux ratio shown in figure 4, has been measured by CALET with high statistical precision, in a wide energy range from 60 GeV/n to ~60 TeV/n [4], using the CALET proton flux published in [16]. Both the statistical (red bars) and the sum of statistical and systematic errors (gray band) are represented. Details on the measurement and the systematic uncertainty calculation can be found in [4] and in its SM. Measurements from other experiments [17] are also included in the same plot.

5. Conclusions

The measurement of the helium spectrum demonstrates the excellent capability of CALET to resolve spectral features in the CR spectra in the large energy range from 40 GeV to 250 TeV. The spectral shape is not consistent with a single power law (at $> 8\ \sigma$ level) and confirms the presence of a hardening above a few hundred GeV, and the onset of a flux softening above a few tens TeV. A DBPL fits both spectral features with parameters that are found to be consistent, within the errors,

with the most recent results of DAMPE [14]. We have also measured the p/He ratio in the interval from 60 GeV/n to ∼60 TeV/n. Our result is found to be in agreement with previous measurements from calorimetric experiments [17] and magnetic spectrometers [4], extending the energy reach with spectrometers by more than one order of magnitude.

6. Acknowledgments

We gratefully acknowledge JAXA's contributions to the development of CALET and to the operations onboard the International Space Station. The CALET effort in Italy is supported by ASI under Agreement No. 2013-018-R.0 and its amendments. The CALET effort in the United States is supported by NASA through Grants No. 80NSSC20K0397, No. 80NSSC20K0399, and No. NNH18ZDA001N-APRA18-0004. This work is supported in part by JSPS Grant-in-Aid for Scientific Research (S) Grant No. 19H05608 in Japan.

References

[1] O. Adriani et al. (CALET Collab.), Astrophys. J. Lett. **863**, 160 (2018).

[2] O. Adriani et al. (CALET Collab.), Astrophys. J. Lett. **829**, L20 (2016).

[3] P. Brogi et al. , PoS (ICRC2021) 101 (2021)

[4] O. Adriani et al. (CALET Collab.), Phys. Rev. Lett. **130**, 171002 (2023).

[5] P. Brogi et al. , PoS (ICRC2015) 595 (2015)

[6] Y. Asaoka et al. (CALET Collab.), Astropart. Phys. **91**, 1 (2017).

[7] O. Adriani et al. (CALET Collab.), Phys. Rev. Lett. **119**, 181101 (2017).

[8] K. Kasahara, Proc. of 24 th ICRC, Vol. 1 (1995) 399 and T. T. Böhlen et al., Nuclear Data Sheets 120 (2014) 211

[9] P. Maestro and N. Mori (for the CALET Collab.), PoS (ICRC2017) 208 (2017).

[10] M. Aguilar et al. (AMS Collab.), Phys. Rev. Lett. **114**, 171103 (2015).

[11] Y. S. Yoon et al., Astrophys. J. **728**, 122 (2011); Astrophys. J. **839**, 5 (2017).

[12] M. Aguilar et al. (AMS Collab.), Phys. Rev. Lett. **115**, 211101 (2015).

[13] G. D'Agostini, Nucl. Instr. and Meth. A 362 (1995) 487 and T. Adye, arXiv:1105.1160v1 (2011)

[14] F. Alemanno et al. (DAMPE Collab.), Phys. Rev. Lett. **126**, 201102 (2021).

[15] M. Aguilar et al. (AMS Collab.), Phys. Rev. Lett. **123**, 181102 (2019).

[16] O. Adriani et al. (CALET Collab.), Phys. Rev. Lett. **129**, 101102 (2022).

[17] Y. S. Yoon et al., Astrophys. J. **839**, 5 (2017) and O. Adriani et al. (PAMELA Collab.), Adv. in Space Res. **51**, 2 (2013) 219.

Full Author List: CALET Collaboration

O. Adriani[1,2], Y. Akaike[3,4], K. Asano[5], Y. Asaoka[5], E. Berti[2,6], G. Bigongiari[7,8], W.R. Binns[9], M. Bongi[1,2], P. Brogi[7,8], A. Bruno[10], N. Cannady[11,12,13], G. Castellini[6], C. Checchia[7,8], M.L. Cherry[14], G. Collazuol[15,16], G.A. de Nolfo[10], K. Ebisawa[17], A.W. Ficklin[14], H. Fuke[17], S. Gonzi[1,2,6], T.G. Guzik[14], T. Hams[11], K. Hibino[18], M. Ichimura[19], K. Ioka[20], W. Ishizaki[5], M.H. Israel[9], K. Kasahara[21], J. Kataoka[22], R. Kataoka[23], Y. Katayose[24], C. Kato[25], N. Kawanaka[20], Y. Kawakubo[14], K. Kobayashi[3,4], K. Kohri[26], H.S. Krawczynski[9], J.F. Krizmanic[12], P. Maestro[7,8], P.S. Marrocchesi[7,8], A.M. Messineo[8,27], J.W. Mitchell[12], S. Miyake[28], A.A. Moiseev[29,12,13], M. Mori[30], N. Mori[2], H.M. Motz[18], K. Munakata[25], S. Nakahira[17], J. Nishimura[17], S. Okuno[18], J.F. Ormes[31], S. Ozawa[32], L. Pacini[2,6], P. Papini[2], B.F. Rauch[9], S.B. Ricciarini[2,6], K. Sakai[11,12,13], T. Sakamoto[33], M. Sasaki[29,12,13], Y. Shimizu[18], A. Shiomi[34], P. Spillantini[1], F. Stolzi[7,8], S. Sugita[33], A. Sulaj[7,8], M. Takita[5], T. Tamura[18], T. Terasawa[5], S. Torii[3], Y. Tsunesada[35,36], Y. Uchihori[37], E. Vannuccini[2], J.P. Wefel[14], K. Yamaoka[38], S. Yanagita[39], A. Yoshida[33], K. Yoshida[21], and W.V. Zober[9]

[1]Department of Physics, University of Florence, Via Sansone, 1 - 50019, Sesto Fiorentino, Italy, [2]INFN Sezione di Firenze, Via Sansone, 1 - 50019, Sesto Fiorentino, Italy, [3]Waseda Research Institute for Science and Engineering, Waseda University, 17 Kikuicho, Shinjuku, Tokyo 162-0044, Japan, [4]JEM Utilization Center, Human Spaceflight Technology Directorate, Japan Aerospace Exploration Agency, 2-1-1 Sengen, Tsukuba, Ibaraki 305-8505, Japan, [5]Institute for Cosmic Ray Research, The University of Tokyo, 5-1-5 Kashiwa-no-Ha, Kashiwa, Chiba 277-8582, Japan, [6]Institute of Applied Physics (IFAC), National Research Council (CNR), Via Madonna del Piano, 10, 50019, Sesto Fiorentino, Italy, [7]Department of Physical Sciences, Earth and Environment, University of Siena, via Roma 56, 53100 Siena, Italy, [8]INFN Sezione di Pisa, Polo Fibonacci, Largo B. Pontecorvo, 3 - 56127 Pisa, Italy, [9]Department of Physics and McDonnell Center for the Space Sciences, Washington University, One Brookings Drive, St. Louis, Missouri 63130-4899, USA, [10]Heliospheric Physics Laboratory, NASA/GSFC, Greenbelt, Maryland 20771, USA, [11]Center for Space Sciences and Technology, University of Maryland, Baltimore County, 1000 Hilltop Circle, Baltimore, Maryland 21250, USA, [12]Astroparticle Physics Laboratory, NASA/GSFC, Greenbelt, Maryland 20771, USA, [13]Center for Research and Exploration in Space Sciences and Technology, NASA/GSFC, Greenbelt, Maryland 20771, USA, [14]Department of Physics and Astronomy, Louisiana State University, 202 Nicholson Hall, Baton Rouge, Louisiana 70803, USA, [15]Department of Physics and Astronomy, University of Padova, Via Marzolo, 8, 35131 Padova, Italy, [16]INFN Sezione di Padova, Via Marzolo, 8, 35131 Padova, Italy, [17]Institute of Space and Astronautical Science, Japan Aerospace Exploration Agency, 3-1-1 Yoshinodai, Chuo, Sagamihara, Kanagawa 252-5210, Japan, [18]Kanagawa University, 3-27-1 Rokkakubashi, Kanagawa, Yokohama, Kanagawa 221-8686, Japan, [19]Faculty of Science and Technology, Graduate School of Science and Technology, Hirosaki University, 3, Bunkyo, Hirosaki, Aomori 036-8561, Japan, [20]Yukawa Institute for Theoretical Physics, Kyoto University, Kitashirakawa Oiwake-cho, Sakyo-ku, Kyoto, 606-8502, Japan, [21]Department of Electronic Information Systems, Shibaura Institute of Technology, 307 Fukasaku, Minuma, Saitama 337-8570, Japan, [22]School of Advanced Science and Engineering, Waseda University, 3-4-1 Okubo, Shinjuku, Tokyo 169-8555, Japan, [23]National Institute of Polar Research, 10-3, Midori-cho, Tachikawa, Tokyo 190-8518, Japan, [24]Faculty of Engineering, Division of Intelligent Systems Engineering, Yokohama National University, 79-5 Tokiwadai, Hodogaya, Yokohama 240-8501, Japan, [25]Faculty of Science, Shinshu University, 3-1-1 Asahi, Matsumoto, Nagano 390-8621, Japan, [26]Institute of Particle and Nuclear Studies, High Energy Accelerator Research Organization, 1-1 Oho, Tsukuba, Ibaraki, 305-0801, Japan, [27]University of Pisa, Polo Fibonacci, Largo B. Pontecorvo, 3 - 56127 Pisa, Italy, [28]Department of Electrical and Electronic Systems Engineering, National Institute of Technology (KOSEN), Ibaraki College, 866 Nakane, Hitachinaka, Ibaraki 312-8508, Japan, [29]Department of Astronomy, University of Maryland, College Park, Maryland 20742, USA, [30]Department of Physical Sciences, College of Science and Engineering, Ritsumeikan University, Shiga 525-8577, Japan, [31]Department of Physics and Astronomy, University of Denver, Physics Building, Room 211, 2112 East Wesley Avenue, Denver, Colorado 80208-6900, USA, [32]Quantum ICT Advanced Development Center, National Institute of Information and Communications Technology, 4-2-1 Nukui-Kitamachi, Koganei, Tokyo 184-8795, Japan, [33]College of Science and Engineering, Department of Physics and Mathematics, Aoyama Gakuin University, 5-10-1 Fuchinobe, Chuo, Sagamihara, Kanagawa 252-5258, Japan, [34]College of Industrial Technology, Nihon University, 1-2-1 Izumi, Narashino, Chiba 275-8575, Japan, [35]Graduate School of Science, Osaka Metropolitan University, Sugimoto, Sumiyoshi, Osaka 558-8585, Japan, [36]Nambu Yoichiro Institute for Theoretical and Experimental Physics, Osaka Metropolitan University, Sugimoto, Sumiyoshi, Osaka 558-8585, Japan, [37]National Institutes for Quantum and Radiation Science and Technology, 4-9-1 Anagawa, Inage, Chiba 263-8555, Japan, [38]Nagoya University, Furo, Chikusa, Nagoya 464-8601, Japan, [39]College of Science, Ibaraki University, 2-1-1 Bunkyo, Mito, Ibaraki 310-8512, Japan